LBL-28908
Preprint

Lawrence Berkeley Laboratory
UNIVERSITY OF CALIFORNIA

Materials & Chemical Sciences Division

National Center for Electron Microscopy

Submitted to Journal of Materials Research

Chemical Structure and Physical Properties of Diamond-Like Amorphous Carbon Films Prepared by Magnetron Sputtering

N.-H. Cho, K.M. Krishnan, D.K. Veirs, M.D. Rubin,
C.B. Hopper, B. Bhushan, and D.B. Bogy

April 1990

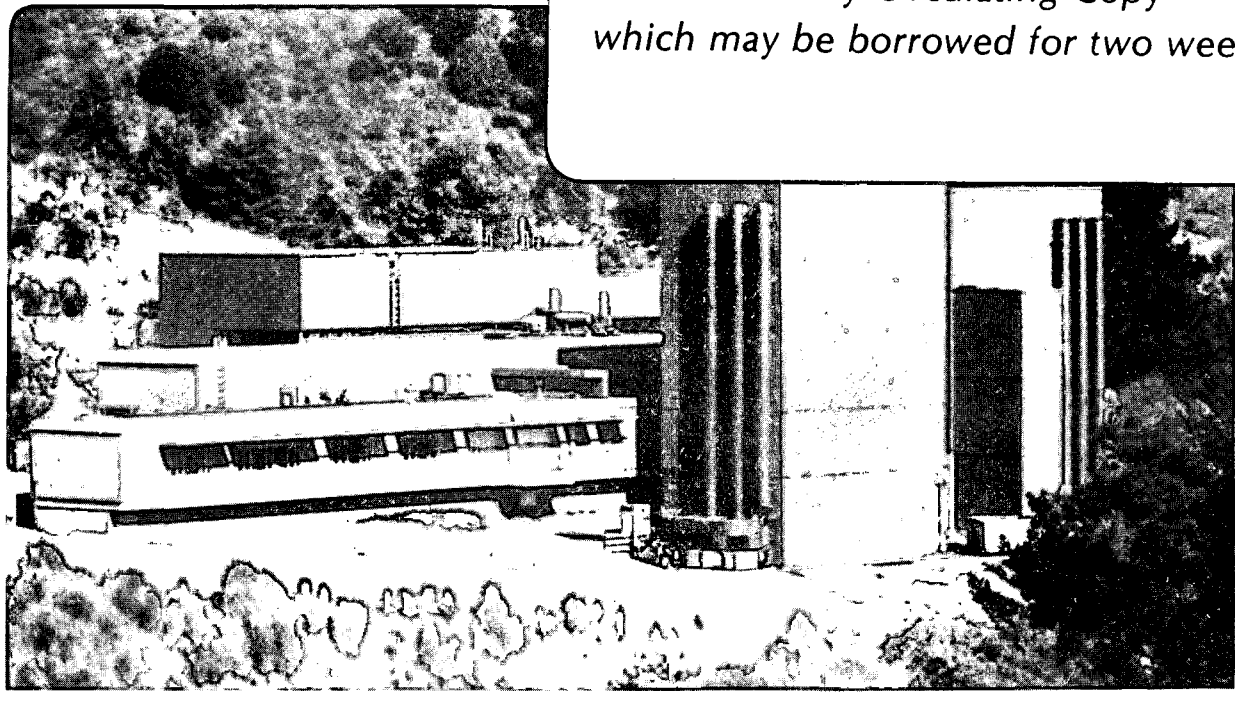

Prepared for the U.S. Department of Energy under Contract Number DE-AC03-76SF00098.

DISCLAIMER

LBL-28908

Chemical Structure and Physical Properties of Diamond-Like Amorphous Carbon Films Prepared by Magnetron Sputtering

N.-H. Cho, K.M. Krishnan, D.K. Veirs, M.D. Rubin,
C.B. Hopper, and B. Bhushan

Lawrence Berkeley Laboratory
University of California
Berkeley, CA 94720

and

D.B. Bogy

Computer Mechanics Laboratory
Dept. of Mechanical Engineering
University of California
Berkeley, CA 94720

This work was supported by the National Science Foundation through Grant MSE-8800149 with the University of California at Berkeley, by the Computer Mechanics Laboratory at UCB, and by the Director, Office of Energy Research, Office of Basic Energy Sciences, Materials Sciences Division, of the U.S. Department of Energy under Contract No. DE-AC03-76SF00098.

CHEMICAL STRUCTURE AND PHYSICAL PROPERTIES OF DIAMOND-LIKE AMORPHOUS CARBON FILMS PREPARED BY MAGNETRON SPUTTERING

N.-H. Cho, K.M. Krishnan, D.K. Veirs, M.D. Rubin, C.B. Hopper,
B.Bhushan*
Lawrence Berkeley Laboratory,
One Cycrotron Road,
Berkeley, CA 94720

D.B. Bogy
Computer Mechanics Laboratory,
Dept. of Mechanical Engineering,
University of California,
Berkeley, CA 94720

ABSTRACT

Thin films of amorphous carbon (a-C) and amorphous hydrogenated carbon (a-C:H) were prepared using magnetron sputtering of a graphite target. The chemical structure of the films were characterized using electron energy loss spectroscopy (EELS) and Raman spectroscopy. The mass density, hardness, residual stress, optical bandgap, and electrical resistivity were determined, and their relation to the film's chemical structure are discussed. It was found that the graphitic component increases with increasing sputtering power density. This is accompanied by a decrease in the electrical resistivity, optical bandgap, mass density and hardness. Increasing the hydrogen content in the sputtering gas mixture results in decreasing hardness (14 GPa to 3 GPa) and mass density, and increasing optical band gap and electrical resistivity. The variation in the physical properties and chemical structures of these films can be explained in terms of the changes in the volume of sp^2-bonded clusters in the a-C films and changes in the termination of the graphitic clusters and sp^3-bonded networks by hydrogen in the a-C:H films.

I. INTRODUCTION

There has been a growing interest in the useful and unique properties of diamond-like amorphous carbon thin films. These properties include high hardness and wear resistivity, chemical inertness, high electrical resistance and lack of magnetic response, optical transparency in the infrared region, and an optical band gap up to a few eV. Amorphous carbon thin films, thus, have potential applications as protective coatings for magnetic and optical disks, wear-resistant coatings for abrasive applications, and also as semiconducting materials.[1-6] These films can be produced by ion beam sputtering, magnetron sputtering and plasma-assisted chemical vapor deposition. Of interest to the computer industry are sputtering techniques using parallel-plate electrodes. These techniques have the advantages of low cost, process simplicity, good process control, and coating homogeneity, and are used routinely for thin film deposition of magnetic media in the production of computer hard disks.

The physical properties of sputtered a-C films change with changes in the deposition parameters. It is important to understand the relation of the chemical structure of a-C thin films to the physical properties in order to define useful deposition parameters. Diamond-like amorphous carbon films are metastable phases formed when carbon particles are condensed on a substrate.[7] A number of investigations have been performed to identify the microstructure of amorphous carbon films using a variety of techniques such as Raman spectroscopy,[8-14] EELS,[9,15-18] nuclear magnetic resonance,[17,19,20] optical measurements,[9,21,23] transmission electron microscopy,[9,24,25] and X-ray photoemission spectroscopy[26]. These studies indicate that the chemical structure and physical properties of the films are

quite variable depending on the deposition techniques and film growth conditions[27]. It is clear that both sp^2- and sp^3-bonded atomic sites are incorporated in diamond-like amorphous carbon films and that the physical and chemical properties of the films depend strongly on their chemical bonding and microstructure.

Carbon has two crystalline forms, graphite and diamond.[28] Graphite, the thermodynamically preferred crystal structure at room temperature, possesses a layer structure; the atoms are strongly bonded within a basal plane (sp^2-hybrid bond), and the planes are weakly bound to one another (van der Waals forces). In diamond, each carbon atom is surrounded by four other carbon atoms and is limited by covalent bonds (sp^3-hybrid bonds) in a tetrahedral structure. In disordered carbon such as pyrolytic carbon,[29-31] the basal planes are compressed and bent; the distance between defectless regions along the a (or b) axis in parallel stacked sheets of graphitic layers is referred to as the crystallite size (L_a) and the stacking height along the c axis is referred to as L_c.

Models of the structure of a-C films have been suggested that attempt to explain the observed high hardness and significant compressive stress.[32-35] For example, random covalent networks of sp^3-, sp^2-hybrid bonded atoms were used in which the bond angles and bond lengths are distorted from their equilibrium positions.[32-34] In some models, hydrogen was incorporated in the films as a network terminator.[35] Medium- or long-range order from the formation of microcrystals dominated by sp^2-bonded atomic sites relieves the compressive stress caused by a constrained random distribution of covalent bonds (sp^2-, and sp^3- hybrid bonds).[36]

There still exist questions concerning the microscopic structure and chemical bonding in diamond-like amorphous carbon thin films. In order

to enhance understanding of this material, it is necessary to investigate how the chemical bonding configurations correlate with the microstructure, and how the microstructure are related to the physical and optical properties. Finally, in order to produce useful films it is necessary to relate the microstructure to the deposition parameters.

In this study, a systematic approach has been taken to investigate how the physical and chemical properties of a-C films vary as a function of two deposition parameters, the sputtering power density and the hydrogen content. Electron energy loss spectroscopy and Raman spectroscopy are used to characterize the chemical bonding and microstructure. Physical properties such as hardness, mass density, residual stress, electrical resistivity, and optical properties are measured and related to the microstructure.

II. EXPERIMENTAL

II.1 Film Preparation

Carbon films were prepared by magnetron sputtering deposition. A 3.0 inch diameter graphite target was attached to the cathode of a magnetron sputtering system and used as a carbon source. The distance between the cathode and substrate surface was about 4.5 cm. An Ar/hydrogen gas mixture was admitted to the discharge chamber. The d.c. power mode was used to ionize the gas mixture at a total pressure of 10 mTorr. No heat was introduced to the substrate from outside; no substrate bias voltage was applied. The deposition rates varied from 0.6 nm/min to 32

nm/min as the sputtering power density changed from 0.1 to 10.0 watts/cm^2.

Two groups of samples were prepared. One group (W-group) of samples was produced under sputtering power densities of 0.1, 1.1, 2.1, and 10.0 watts/cm^2. These samples are called W1, W2, W3, and W4, respectively, in this paper. For these samples, pure Ar gas was introduced to the chamber, which then formed a plasma of Ar^+ ions and electrons when negative voltage was applied to the cathode. The other group (H-group) of samples was prepared with various hydrogen concentrations (0.5, 1.0, 3.0, 6.0, 10.0, and 15.0%) in the sputtering gas mixture with Ar as the major species. These samples are called H1, H2, H3, H4, H5, and H6, respectively, in this paper. The sputtering power density was kept at 2.1 watts/cm^2 for all H-group samples; the other deposition parameters were held constant.

NaCl, Si wafer, and silica glass were used as substrates. Carbon films with a thickness of about 300 Å deposited on NaCl were used for TEM and Raman spectroscopy studies. For the TEM studies, the films grown on NaCl crystals were floated off in distilled water and mounted on copper grids. One micron thick carbon films on Si were used for the measurement of hardness and mass density. The Si substrates were cleaned with 48-52% HF acid for about 5 min to remove any oxide layer or other contaminants. The cleaned wafer was put into the vacuum chamber as soon as possible. We found that cleaning the wafers improved the adhesion.

II.2 Film Characterization

Electron energy loss spectra were obtained using a JEOL 200 CX electron microscope operating at 200 kV. A parallel electron energy loss spectrometer (Gatan 666) and a Kevex multichannel analyzer were used to acquire and analyze the EELS data. The overall energy resolution (the FWHM of the zero-loss peak) was about 1.2 eV. The resolution was limited by the thermal spread of the electrons emitted by the LaB_6 filament; better energy resolution could only be achieved by a significant compromise of the beam intensity. The specimen area from which the spectra were obtained was about 150 nm in diameter. Collection time for each spectrum was about 20-30 seconds. The electron beam intensity was reduced for recording the low-energy EELS spectra (< 50 eV) to prevent saturation of the diode counting array. At the backfocal plane, an objective aperture (20 μm in diameter) was inserted to prevent the transmitted electrons, which experience large angle scattering in the specimen, from contributing to the spectra. The low-energy EELS spectra for all samples were recorded from regions with nearly the same thickness (about 900 Å).

Raman spectra were obtained in a backscattering geometry from thin films deposited on NaCl substrates, using the 488 nm Ar^+ laser line at a power of 30 to 150 mW. The Raman apparatus has been described previously,[9] and will be described briefly here. All the measurements in this study were carried out at room temperature. The Raman scattered light was collected with a f/1.3 50 mm camera lens and focused onto the entrance slit of a 0.64 m single monochromator. A six-cavity interference filter was used to select the wavelength region of interest. Raman spectra in the 1000 cm^{-1} to 2000 cm^{-1} range were obtained and analyzed, fitting to the

sum of two Gaussian line shapes and a linear background term. The line positions obtained from the fit have a standard error of 3 cm^{-1} (2σ).

Secondary ion mass spectrometry (SIMS) data were taken from the carbon films deposited on Si substrates using a Perkin-Elmer SIMS instrument. Five keV Ar^+ ions were used to erode the film surface, rastering an area of 3x3 mm^2 with a linear gain rate of 40%. SIMS spectra were obtained in the range of 1 to 100 m/e from each sample under the same measurement conditions to determine qualitatively the composition (mainly hydrogen content).

II.3 Physical Properties

The electrical resistivity of the films was measured using the four-point probe method. A specific electrical current is produced between two outside probes, and the resistivity is determined from the voltage drop across two inside probes and the thickness of the films. The upper limit of the instrument used for this measurement was 10^6 Ω cm.

The mass density of each film was determined by measuring its weight and volume. A step between a film-covered area and an area without film was made by placing a mask when films were grown. The step height equivalent to the film thickness was measured with a stylus profiler. The typical thickness was about 1.0 μm. The volume of the films was determined from the film thickness and the area. The net weight of each film was determined from the difference between the weight of the substrate before deposition and the weight of the substrate with a film after deposition. The net weight was typically about $1.0x10^{-3}$ g; the resolution of the balance was of 10^{-5} g.

The hardness of the films was determined with a nanoindentor (produced by Nano Instruments Inc.). In this measurement, the capacitance displacement gauge detects the plastic depth (displacement) with an accuracy of 0.2-0.3 nm. The force resolution of the system is about 0.5 μN. Elastic displacement components were measured after unloading, and the total displacement was used to determine the hardness.

Optical measurements were carried out on films deposited on glass microscope slides. Reflection and transmittance measurements were performed over near ultraviolet, visible and near-infrared wavelengths from 180 to 2500 nm using a Perkin Elmer Lambda 3 spectrophotometer. The details in the measurements and results have been described elsewhere.[37]

Internal stresses of the films were determined by a beam-bending technique.[38] The bending curvatures of 0.3 mm thick Si substrates were measured with a stylus profiler before and after deposition of films ~1μm in thickness. The curvature obtained before deposition was subtracted from the curvature obtained after deposition, resulting in a net curvature due to the films stress. A detailed description for the measurement and results is available elsewhere.[37]

III. RESULTS

III.1 EELS

EELS spectra from polycrystalline graphite and single crystal diamond in an energy range up to 50 eV are shown in Fig. 1. Two

prominent peaks are seen at 27.0 eV and 6.5 eV in graphite, while one peak is observed at 35 eV in diamond. A 'hump' is also seen at 25.0 eV in diamond, and no peaks are observed below 10 eV. The two prominent peaks seen in the low EELS spectra (<50 eV) of graphite correspond to the energy loss of incident electrons by bulk plasmon excitations. The peak at 6.5 eV is attributed to the plasmon oscillation of the π electrons in the valence band;[39,40] the peak at 27 eV represents the collective excitation of all the valence ($\pi+\sigma$) electrons. In graphite, the peaks at 6.4 and 27.0 eV are called π and $\pi+\sigma$ peaks, respectively. The peak at 35 eV in diamond appears at a higher energy region compared to the peak at 27 eV in graphite. The plasmon frequency of diamond is higher than that of graphite due to the higher valence electron density.[41] The presence of a little hump at 25 eV in the spectrum for diamond may result from sp^2-bonded carbon at the surface of the diamond specimen due to electron beam damage.

Fig. 2 shows the EELS spectra from W-group carbon films; spectra a, b, c, and d were obtained from samples W1, W2, W3, and W4, respectively. The $\pi+\sigma$ peak in each spectrum is found at nearly the same energy level (24.5 ± 0.1 eV), lower in energy than that of graphite (27 eV). The π peak positions in the spectra for samples W1, W2, W3, and W4 are 5.0, 5.5, 6.1, and 6.0 eV, respectively; also lower in energy than that of graphite (6.4 eV).

H-group EELS spectra are shown in Fig. 2; spectra e, f, g, and h were taken from samples H1, H3, H5, and H6, respectively. The $\pi+\sigma$ peak in spectrum e is seen at 23.3 eV, and in spectra f, g, and h at around 22.4 eV. The $\pi+\sigma$ peaks in the spectra of H-group samples are found at lower energy compared to the corresponding peaks in the spectra of W-group samples. The π peak positions for samples H1, H3, H5, and H6 are 6.5, 6.7, 6.1, and 5.8 eV, respectively. The π peaks for samples H1 and H2 are found at nearly

the same energy. In general, the peak positions are observed to shift to lower energy as the hydrogen content of the sputtering gas mixture increases beyond 3 %. The peaks in the 5-8 eV region in Fig. 2 are less intense compared to that of graphite in Fig. 1.

Figure 3 shows the EELS spectra associated with the inner-shell (K-shell) ionization. Spectra a and b were obtained from diamond and graphite, respectively. Sharp peaks are observed at 285.5 eV and 292.5 eV in graphite, while no peak is seen at 285.5 eV in diamond. The general features of the K-shell EELS spectra for the W- and H-group carbon samples resemble the features of graphite; the structure of the former looks like a smeared structure of the latter. The K-shell EELS spectra reflect the conduction band Density of States (DOS) with a transition probability weighting factor.[42,43] The peak at 285.5 eV in the spectra is generated by the excitation of electrons in the K edge to the π^* conduction band. Spectra c, d, e, and f were obtained from samples W1, W4, H3, and H6, respectively. All these spectra exhibit a peak at 285.5 eV, similar to the spectra of graphite. However, it is noticed that graphite has a more intense peak at 285.5 eV than the carbon thin films. The peak intensity at 285.5 eV decreases as the hydrogen content of sputtering gas mixture increases beyond 3%. The spectra obtained from the a-C films show a relatively broad peak in the energy range above 287 eV in comparison to the sharp peaks seen in diamond.

III.2 Raman Spectroscopy

Raman spectra from a single crystal of diamond and polycrystalline graphite are shown in Fig. 4. A sharp peak is seen at 1332 cm^{-1} in diamond.

Two peaks are observed at 1580 cm^{-1} (G-band) and 1358 cm^{-1} (D-band) in graphite; the integrated ratio (I_d/I_g) of the D band to the G band was determined to be 0.69. The peak at 1580 cm^{-1} in graphite is due to the Raman allowed E_{2g} mode.[44] The peak at about 1350 cm^{-1} in polycrystalline graphite results from a relaxation of the **k**=0 selection rule for Raman scattering in crystals.[12]

Figure 5 shows the details of the Raman spectra between 1000 cm^{-1} and 2000 cm^{-1} obtained from W- and H-group samples. The abscissa indicates the frequency shift (in wavenumbers) from the Rayleigh line. Spectra a, b, c, and d were taken from samples W1, W2, W3, and W4, respectively. It is seen that the shape of the experimental curves vary as a function of sputtering power density. In particular, a significant change in the peak shape occurs at low sputtering power densities (below 1.1 eV).

The experimental data are fit best by two peaks with Gaussian line shapes and a linear background; each plot consists of the experimental data and the fitted curves. From the fitting parameters, the peak position, peak width, and integrated intensity ratio of the two peaks are obtained. .

Tuinstra and Koenig have shown that the Raman spectra of disordered graphite changes smoothly as the amount of disorder increases. In their experiments, the measure of disorder is the crystallite size, L_a, measured in X-ray diffraction experiments. As L_a decreases the **k**=0 selection rule for Raman scattering in crystals is relaxed. In the limit of an amorphous material all normal modes are allowed and the Raman spectra becomes a measure of the phonon density of states weighted by a matrix element.[45] The two peaks observed in these experiments correspond to maxima in the phonon density of states of the material. We use the nomenclature of the D-band and G-band that has been used to describe

disordered graphite and amorphous carbon films. We note that the origin of the intensity of the G-band in a-C is not the sharp, Raman-allowed E_{2g} mode observed in graphite.[46]

Table 1 shows all the fitting parameters for the spectra illustrated in Fig. 5. Two important features can be noticed: (1) the G-band position shifts to a lower frequency as the sputtering power density decreases from 10.0 to 0.1 watts/cm^2; (2) the intensity ratio I_d/I_g also decreases from 5.65 to 1.85 as power density decreases from 10.0 to 0.1 watts/cm^2. In addition, the G and D band width for sample W1 appears to be much smaller than the band widths obtained from the other samples.

Raman spectra were also obtained from H-group samples. Spectra e, f, and g were recorded from samples H1, H2, and H3, respectively. The Raman spectrum for sample H1 appears similar to the Raman spectrum for sample W1. The G band is found at nearly the same frequency (1541 cm^{-1}). However, the full width at half maximum (FWHM) of the D band and the integrated intensity ratio (I_d/I_g) of this peak are smaller than those for sample W1. For sample H2, two prominent peaks are seen at 1579 and 1345 cm^{-1}. A strong fluorescence is observed in sample H3 masking the Raman spectrum; this fluorescence prevented Raman spectra to be observed in samples H3 through H6.

III.3 SIMS

Figure 6a illustrates a typical SIMS survey for sample W3. The vertical lines indicate the intensity of each species (m/e) in logarithmic scale. Hydrogen, carbon clusters, and hydrogen-bound carbons are observed in this spectrum. In SIMS measurements, the sputtered species

can be neutral atoms, atomic ions (positive or negative, singly and multiply charged) or clusters. The surface conditions affect the sputtering process and the distribution of the sputtered species.[47]

A qualitative comparison of the hydrogen content in each film was performed assuming that variations in the carbon film surface do not affect the sputtering process for W-group and samples H1 and H2. The intensity ratio of the H^+ to the C^+ was measured for each sample; the results are illustrated in Fig. 6b. The ratio is constant at 0.2 ± 0.05 for the W-group samples. In contrast, a significant difference is observed in the ratio between a-C films (W-group samples) and a-C:H films (H-group samples). Sample H2 exhibits a ratio of 1.1 ± 0.1.

III.4 Physical Properties

The electrical resistivity of the films grown at various sputtering power densities is shown in Fig. 7. A rapid decrease is observed in the electrical resistivity at a low sputtering power density level (below 1.1 watts/cm^2). Above this power density, little variation is found as a function of sputtering power density. Electrical resistivity was also measured for the H-group samples. Sample H2 has a resistivity of 10^5 Ω cm and the other H-group samples exhibit a resistivity higher than 10^6 Ω cm (the maximum range of the instrument).

The optical band gap of each sample was calculated from the energy dependence of the optical absorption coefficient. The gap (E_g) was determined from the extrapolated intercept of a linear fit to $(\alpha h\nu)^{1/2}$ vs. $h\nu$ (the photon energy).[48] The gap consistently decreases from 0.7 to 0.4 eV, as the sputtering power density increases from 0.1 to 10.0 watts/cm^2. For the a-

C:H films, the gap consistently increases from 0.45 to 2.12 eV as the hydrogen content of the sputtering gas mixture increases from 0 to 10%.

The mass density of the films is shown in Fig. 8. The mass density of sample W1 was determined to be 2.1 g/cm^3. As the sputtering power density increases, the mass density decreases to 1.8 g/cm^3 at 10.0 watts/cm^2. The mass density of H-group samples varies in the range of 1.7 to 1.6 g/cm^3 as the hydrogen content changes from 1 through 10%, Table 2.

The hardness data of W- and H-group samples are illustrated in Fig. 9. For the a-C films, samples W1 and W2 exhibit nearly the same hardness of around 15±1.25 GPa. At higher sputtering power densities the hardness decreases to 12±1.25 GPa for sample W4. The elastic modulus of the films, Table 2, also decreases with sputtering power density, from 140 GPa to 115 GPa for samples W1 and W4, respectively.

For the a-C:H films, the hardness of the films decreases from 14 GPa to 3 GPa as the hydrogen content of the sputtering gas mixture increases from 0.5 to 6%; above 6%, the hardness increases slightly. The elastic modulus of these samples is observed to vary in the same way as the hardness.

The residual stress of the a-C films does not vary as a function of sputtering power density. On the other hand, the residual stress decreases significantly with initial increases in the hydrogen content of the sputtering gas mixture. In particular, carbon films prepared with a hydrogen content of 0.5% in the sputtering gas mixture exhibit such high residual stress that at a thickness of about 1 μm delamination occured.

IV. DISCUSSION

IV.1 Chemical Bonding and Microstructure of the a-C Films

The observation of the π^* peak at 285.5 eV in the EELS spectra indicates that sp^2-bonded atomic sites are present in the a-C films. The peaks at energy levels between 5 and 6 eV in the low-energy EELS spectra of W-group samples are analogous to the peak at 6.4 eV in graphite.[15,39] The presence of these peaks in Fig. 2 is also attributed to the π electrons in the valence band. In other words, sp^2-bonded atomic sites are present.

The peak positions in low-energy EELS are associated with the plasmon oscillation of the valence electrons, and have a characteristic frequency of $\omega_p = (ne^2/\varepsilon m)^{1/2}$ (where, n=density of free electrons, ε=permittivity of free space, m=electron mass, and e=electron charge). The energy lost by the electrons in exciting the plasmons is determined, to a first approximation, by $\Delta E = h\,(ne/\varepsilon m)^{1/2}$ (where, h=Plank constant) and are related to the electron density. Plasmon peaks are seen at different energies for amorphous carbon films grown by different deposition methods.[49] The $\pi+\sigma$ peak positions (24.6 ± 0.1 eV) of W-group samples indicate that the electron density in the valence band of these films is lower than that of graphite (27 eV). However, within the range of applied sputtering power densities, there seems to be no significant variation in the valence electron density of the W-group films.

The increase in sputtering power density from 0.1 to 10.0 watts/cm^2 results in the π peak position moving from 5.0 to 6.0 eV. As the peak position is quadratically proportional to the density of the π electrons in the

valence band, there is an increase in the number of sp^2-bonded atomic sites as the sputtering power density increases.

From SIMS measurements, the lack of variation in the H^+/C^+ ratio as a function of sputtering power density for W-group samples confirms that samples W1-W4 contain the same amount of hydrogen. Therefore, for the W-group samples, the possibility can be ruled out that the significant differences in the sputtering time required to deposit films of an equal thickness at the different sputtering power densities results in a difference in the hydrogen content of the film. The comparison of the SIMS data of W-group with those of H-group samples indicates a signigicant difference in the hydrogen content between the two groups.

The Raman spectra of the carbon samples are analyzed in terms of band position, integrated intensity ratio, and bandwidth of the G- and D-bands.[10-14,44] In a theoretical study, Beeman et al modeled bulk amorphous carbon using increasing amount of bond angle disorder and four-fold coordination. It was found that increasing the number of sp^3-bonded atomic sites leads to lower frequencies instead of a mixture of the Raman peaks associated with diamond and graphite.[14] Richter et al calculated the frequency of the G-band using a simple valence force model weighted by the fraction of sp^3 to sp^2 bonds. They found that frequency shifts in the G-band are only caused by changes in the force constants and correspond to a certain sp^3 bonding fraction.[13]

Consequently, the shift of the G band to lower frequency with the decrease in sputtering power density is consistent with an increase in the number of sp^3-bonded atomic sites. In particular, the rapid increase in the G-band Raman frequency seen in the power density data below 1.1 watts/cm^2 suggests that the sp^2/sp^3 ratio increases significantly with

increasing sputtering power density. The range of the observed frequency shift for the G-band corresponds to a sp^3-bonding fraction of 4 to 15% in the model of Richter et al.[13]

From the Raman spectroscopy of graphitic carbon, it has been shown that the intensity of the D-band is inversely proportional to the effective crystallite size (L_a) in the direction of the graphite basal plane and that a linear relationship between I_d/I_g and $1/L_a$ exists (L_a was obtained from X-ray data).[44] At the smallest L_a observed, L_a=2.7 nm, the intensity ratio was I_d/I_g=1.1. Some studies have suggested that I_d/I_g ratio greater than 1.1 observed in a-C thin films are unreliable for obtaining microcrystallite size.[10] All the samples in this study have I_d/I_g much greater than 1.1. Therefore 2.7 nm is an upper limit on the crystallite size L_a. The presence of the optical gap (E_g) in the a-C films however, indicates that the domains of sp^2-bonded carbon are finite in size and that some medium-ranged order of the sp^2 clusters exists.[45] The observed optical band gap (0.7-0.4 eV) for a-C films, similar to that of evaporated a-C, indicates that these films contain sp^2-bonded clusters with L_a of ~15 Å.[21]

IV.2 Hydrogen Effects

The effect of hydrogen on the chemical bonding and microstructure of diamond-like a-C:H films can be understood by comparing the EELS and Raman spectra of samples H1-H6 with that of sample W3; all these samples were prepared at the same condition except for the hydrogen content.

The $\pi+\sigma$ peaks in the EELS spectra of H-group samples are found at a lower energy level, compared to the corresponding peaks in the spectra of W-group samples. The difference in the $\pi+\sigma$ peak positions between the two

groups agrees well with the lower mass density found in the H-group films (~1.6 g/cm^3) , as compared to that of W-group films (2.0 g/cm^3). However, the π peak positions indicate that the density of π electrons in the a-C:H films is higher than the density of π electrons in the a-C films. The observed G-band position at near 1579 cm^{-1} for sample H2 also indicates that sp^2-bonding fraction has increased with the incorporation of hydrogen in a-C:H films. The density of π electrons varies with the hydrogen content; the number of sp^2-bonded atomic sites decreases as the hydrogen content of the sputtering gas mixture increases beyond 3%. It is also found that the π^* peaks in the K-shell EELS spectra look more intense for the samples that have a higher density of π electrons as determined from their plasmon frequency. In particular, sample H3 exhibits the largest intensity ratio of the π^* peak to the σ^* peak, and this ratio decreases as the hydrogen content of the sputtering gas mixture increases.

Increasing the hydrogen content of the sputtering gas mixture results in changes in the Raman spectra of the a-C:H films. A rapid rise in fluorescence is observed that limits the ability to observe a Raman spectrum in samples H3 through H6. For samples H1 and H2, the bandwidth decreases, the I_d/I_g ratio decreases, and the band positions increase compared to the Raman spectra for sample W3. These changes in the Raman spectra of a-C:H films are consistent with the growth of graphitic microcrystallites; the Raman spectrum of H2 minus the substantial fluorescence background is quite similar to the Raman spectrum of L_a~30Å graphite microcrystallites reported by Lespade et al.[11] The crystallite size is larger than the sp^2-bonded clusters that are expected to be present in a-C films from their optical properties. Hydrogen incorporation in the films enhances the crystallinity of the sp^2-bonded clusters and also increases the

sp^2-bonding fraction in the films. The fluorescence probably arises from π-bonded carbon clusters bounded by hydrogen.[50]

IV.3 Physical Properties

The change in the electrical conductivity over a small sputtering power density range (0.1-1.1 Watts/cm^2) coincides with a rapid change in the results of Raman spectroscopy and EELS. The decrease in the electrical resistivity and the optical band gap of W-group samples with increasing sputtering power density is attributed to an increase in the number of sp^2-bonded atomic sites. The increase in the total number of sp^2-bonded atomic sites results in a reduction of the gap between the π and π* bands.

The overall increase in the sp^3-bonding fraction at lower sputtering power density is believed to contribute to the increase in the electrical resistivity and optical band gap by increasing the gap between π and π* bands. In contrast, the a-C:H films that appear to contain a higher sp^2-bonding fraction than the a-C films have higher electrical resistivity. The high electrical resistivity (> 10^6 Ω cm) of H-group samples may result from changes in the microscopic morphology of the films due to hydrogen. It is controversial whether hydrogen preferentially bonds to specific atomic sites (sp^2- or sp^3-bonded) or not.[51,52] However, incorporation of hydrogen in the amorphous carbon should result in terminating (C-C) sp^3-bonded networks as well as reducing the bonding between graphitic clusters and surrounding sp^3-bonded networks. Such termination will result in a decrease in the mobility of the electrons. The presence of disconnected sp^2-bonded clusters and terminated C-C sp^3-bonded networks results in a considerable decrease in the electrical conductivity, hardness, and internal

stress of the H-group samples. Similar variation in the hardness, density, and chemical bonding configurations (sp^2/sp^3) with hydrogen content was reported by Jansen et al. for hydrogenated carbon.[19]

The volume associated with the graphitic components (sp^2-bonded atomic sites) becomes larger as the sputtering power density increases. If the remainder of the film is random sp^3-bonded atomic sites, then the mass density of the films should decrease with the increase in the total fraction of graphite component. However, the mass density (2.1-1.7 g/cm^3) for the a-C films is smaller than that of graphite (2.27 g/cm^3), indicating that a relatively open structure may be present in the carbon films. By open structure we mean the presence of atomic scale voids which are larger than the spacing among regular atomic arrangements. The variation in the mass density of the W-group samples implies that the volume associated with the open structure increases with sputtering power density.

The carbon films prepared at a higher sputtering power density contain more sp^2-bonded carbon than the films grown at lower power density. The proposed open structure may result from voids between graphitic layers and/or the boundaries of graphitic microcrystals that are filled by random sp^3-bonded atomic sites. If the amorphous carbon possesses relatively large sp^2-bonded clusters, then the increase in the interface area should play an important role in the mass density. In particular, for graphitic microcrystals of a few nm in diameter, the atomic arrangements at interfaces between the sp^2-bonded clusters and the sp^3-bonded random networks will affect considerably the mass density and hardness of the films. The hardness of the a-C films (15-11 GPa) is comparable to the knoop hardness of a-C:H films (1250-1650 HK) deposited

from benzene vapor in a rf plasma;[3] these hardnesses are about 8-9 in Mohs scale.

The mass density of H-group samples (1.6-1.7 g/cm^3) is lower than that of W-group samples (2.1-1.8 g/cm^3), and consistently decreases as the hydrogen content of the sputtering gas mixture increases. This suggested that hydrogen terminates sp^2-bonded clusters, thereby increasing the number and extent of atomic scale voids at the cluster interfaces. Hydrogen-terminated sp^2-bonded clusters are consistent with the Raman, hardness, and electrical resistivity results. The mass density of the H-group samples is in the same range reported previouly for a-C:H films[3,27]. It is of interest to note that the hydrogenated amorphous carbon films show a remarkably wide range of hardness (3-60 GPa) depending on the deposition conditions.[45] In our study, hardness could not be measured for the a-C:H films prepared at low hydrogen contents (<1%) due to the film delamination caused by high stress.

V. SUMMARY

Two groups of amorphous carbon films prepared by magnetron sputtering were investigated. Changes in the sputtering power density and the hydrogen content in the sputtering gas mixture resulted in systematic changes in the physical properties, EELS, Raman spectroscopy measurements of these films. We interprete these results as a systematic variation in the chemical structure of the amorphous carbon films as a function of the deposition parameters..

The a-C films were studied as a function of sputtering power density. Results from EELS and Raman spectroscopy suggest that the sp^2 bonding fraction increases with increasing sputtering power density. The electrical resistivity and the optical band gap of the a-C films decrease with increasing sputtering power density. The mass density of the a-C films is lower than that of graphite, and decreases as sputtering power density increases, indicating that open structure is accompanied by sp^2-bonded clusters in the a-C films. Increasing the sputtering power density results in the increase in both the sp^2 bonding fraction and the extent of voids in a-C films.

The a-C:H films have higher electrical resistivity and lower mass density than the a-C films. This difference in physical properties is related to the microstructure of the a-C:H films. Incorporation of hydrogen results in terminating sp^2-bonded clusters and sp^3-bonded networks, and causes a decrease in electron mobility and an increase in the number and extent of atomic scale voids in the films. The decrease in hardness, internal stress and mass density of a-C:H films with the hydrogen content of the sputtering gas mixture are consistent with the above microstructural model for these films.

The systematic change in the mass density , electrical resistivity, optical band gap, hardness and residual stress with the deposition parameters in these experiments are interpreted using a model for the structure of amorphous carbon, in which amorphous carbon consists of sp^2-bonded clusters and sp^3-bonded random networks. The changes in the volume of sp^2-bonded clusters due to sputtering power density and in the termination of the sp^2-bonded clusters and sp^3-bonded networks due to

hydrogen incorporation in the films explain the systematic changes in the properties.

VI. ACKNOWLEDGMENTS

The authors would like to thank Mr. C.J. Echer for assistance in using the microscope facilities at the National Center for Electron Microscopy, and R.L. White for performing the hardness measurements. This work was supported by the National Science Foundarion through Grant MSE-8800149 with the Univ. of Cal. at Berkeley, by the Computer Mechanics Laboratory at UCB, and by the Director, Office of Energy Research, Office of Basic Energy Sciences, Materials Sciences Division, of the U.S. Department of Energy under Contract No. DE-AC03-76SF00098.

*On sabbatical leave from IBM Research Division, Almaden Research Center, San Jose, CA 95120

VII. REFERENCES

1. B. Meyerson and F.W. Smith, J. Non-Cryst. Solids, **35/36**, 435, 1980.

2. L.P. Andersson, Thin Solid Films, **86**, 193, 1981.

3. A. Bubenzer, B. Dischler, G. Brandt, and P. Koidl, J. Appl. Phys. **54**, 4590, 1983.

4. T. Mori and Y. Namba, J. Vac. Sci. Technol., **A1**, 23, 1983.

5. D.R. McKenzie, R.C. McPhedran, L.C. Botten, N. Savvides, and R.P. Netterfield, Appl. Opt., **21**, 3615, 1982.

6. H. Kurokawa, T. Mitani, and T. Yonezawa, IEEE Transactions on Magnetics, Mag-**23**, 5, 1987.

7. C. Weissmantel, Proc. EMRS Meet., 49, 1987.

8. R.P. Vidano and D.B. Fischbach, Solid State Commun., **39**, 341, 1981.

9. H.-C. Tsai, D.B. Bogy, M.K. Kundmann, D.K. Veirs, M.R. Hilton, and S.T. Meyer, J. Vac. Sci. Technol. **A6**, 2307, 1988.

10. C. Beny-Bassez, and J.N. Rovzavd, Scanning Electron Microscopy, 119, 1985.

11. P. Lespade, R. Al-Jishi, and M.S. Dresselhaus, Carbon, **20**(5), 427, 1982.

12. M. Nakamizo, R. Kammereck, and P.L. Walker, Carbon, **12**, 259, 1974.

13. A. Richter, H.-J. Scheibe, W. Pompe, K.-W. Brzezinka, and I. Muhling, J. Non-Cryst. Solids, **88**, 131, 1986.

14. D. Beeman, J. Silverman, R. Lynds, and M.R. Anderson, Phys. Rev., **B30**, 870, 1984.

15. J. Fink, T. Muller-Heinzerling, J. Pfluger, A. Bubenzer, P. Koidl, and G. Crecelius, Solid St. Commun., **47**, 887, 1983.

16. J. Fink, T. Muller-Heinzerling, J. Pfluger, B. Dischler, D. Koidl, A. Bubenzer, and R.E. San, Phys. Rev., **B30**, 4713, 1984.

17. R. H. Jarman, G.J. Ray, R.W. Stanley, and G.W. Izajac, Appl. Phys. Lett. **49**(17), 1065, 1986.

18. C. Gao, Y.Y. Wang, A.L. Ritter, and J.R. Dennison, Phys. Rev. Lett. **62**(8), 945, 1989.

19.F. Jansen, M. Machonkin, S. Kaplan, and S. Hark, J. Vac. Sci. Technol., **A3**(3), 605, 1985.

20. A. Grill, B.S. Meyserson, V.V. Patel, J.A. Reimer, and M.A. Petrich, J. Appl. Phys., **61**(8), 2874, 1987.

21. F.W. Smith, J. Appl. Phys., **55**(3), 764, 1984.

22. D.R. McKenzie, R.C. McPhedran, N. Savvides, and L.C. Bolten, Phil. Mag., **48**, 341, 1983.

23. N.J. Zaluzec, Ultramicroscopy, **9**, 319, 1982.

24. H. Vora and T.J. Moravec, J. Appl. Phys., **52**(10), 6151, 1981.

25. C. Weissmantel, Thin Solid Films, **58**, 101, 1979.

26. F.R. McFeely, S.P. Kowlaczyk, L. Ley, R.G. Cavell, R.A. Pollak, and D.A. Shirley, Phys. Rev., **B9**, 5268, 1974.

27. H. Tsai and D.B. Bogy, J. Vac. Sci. Technol., **A5**(6), 3287, 1987.

28. L. Pauling, The Nature of the Chemical Bond, third ed., Cornell Univ. press.

29. B.E. Warren, Phys. Rev., **9**, 693, 1941.

30. R.E. Franklin, Proc. Roy. Soc., **A209**, 196, 1951.

31. G.M. Jenkins, K. Kawamura, and L. Ban, Proc. Roy. Soc., **A327**, 501, 1972.

32. B.J. Stenhouse and P.J. Grout, J. Non-Crystalline Solids, **27**, 247, 1978.

33. D. Beeman, J. Silverman, R. Lynds, and M.R. Anderson, Phys. Rev., **B30**, 870, 1984.

34. J.C. Phillips, Phys. Rev. Lett., **42**, 153, 1979.

35. J.C. Angus and F. Jansen, J. Vac. Sci. Technol., **A6**, 1778, 1988.

36. J.C. Angus and C.C. Hayman, Science, **241**, 913, 1988.

37. M. Rubin, C.B. Hopper, N.-H. Cho, and B. Bhushan, J. Materials Research 1990 (submitted).

38. R.J. Jaccodine and W.A. Schlegee, J. Appl. Phys., **37**(6), 2429, 1966.

39. W.Y. Liang and S. Cundy, Phil. Mag., **19**, 1031, 1969.

40. E.A. Taft and H.R. Phillip, Phys. Rev., **138**, A197, 1965.

41. R.F. Egerton and M.J. Whelan, Phil. Mag., **30**, 739, 1974.

42. R.F. Egerton and M.J. Whelan, J. Electron Spectrosc. Rel. Phenom., **3**, 232, 1974.

43. A. Koma and K. Miki, Appl. Phys., **A34**, 35, 1984.

44. F. Tuinstra and J.L. Koenig, J. Chem. Phys., **53**, 1126, 1970.

45. J. Robertson, Advances in Physics, **35**, 317, 1986.

46. R. Al-Jishi, and G. Dresselhaus, Phys. Rev. **B26**, 4514, 1982.

47. L.C. Feldman, and J.W. Mayer, Fundamentals of Surface and Thin Films Analysis, North Holland, Amsterdam, 1986.

48. J. Tauc, R. Grigorovic, and A. Vancu, Phys. Status Solids, **15**, 627, 1966.

49. W. Scharff, K. Hammer, O. Stenzel, J. Ullman, M. Vogel, T. Frauenheim, B. Eibisch, S. Roth, S. Schulze, and I. Muhling, Thin Solid Films, **171**, 157, 1989.

50. J. Robertson, and E.P. O'Reilly, Phys. Rev., **B35**, 2946, 1987.

51. B. Dischler, A. Bubenzer, and P. Koidl, Solid St. Commun., **48**, 105, 1983.

52. M.P. Nadler, T.N. Donovan, and A.K. Greene, Appl. Surf. Sci., **18**, 10, 1984.

FIGURE CAPTIONS

Fig. 1. Electron energy loss spectrum in the plasmon region: (a) diamond; (b) graphite.

Fig. 2. Low electron energy loss spectra for W- and H-group samples: (a) sample W1; (b) sample W2; (c) sample W3; (d) sample W4; (e) sample H1; (f) sample H3; (g) sample H5; (h) sample H6.

Fig. 3. High electron energy loss spectra of different carbon samples: (a) diamond; (b) graphite; (c) sample W1; (d) sample W4; (e) sample H3; (f) sample H6.

Fig. 4. Raman spectra for diamond (a) and graphite (b).

Fig. 5. Raman spectra of different carbon samples. The experimental data and fit are illustrated: (a) sample W1; (b) sample W2; (c) sample W3; (d) sample W4; (e) sample H1; (f) sample H2; (g) sample H3.

Fig. 6. (a) Secondary ion mass spectra of a diamond-like carbon film prepared at 2.1 watts/cm^2. (b) Open circles represent intensity ratio (H^+/C^+) of the SIMS data for diamond-like carbon films prepared at 0.1, 1.1, 2.1, and 10.0 watts/cm^2; a closed circle represents the ratio for sample H2.

Fig. 7. Electrical resistivity of the diamond-like carbon films vs sputtering power density.

Fig. 8. Mass density of W- and H-group samples; open and closed circles represent the mass density of the a-C films (W-group) and of the a-C:H films (H-group), respectively.

Fig. 9. Hardness of W- and H-group samples; open and closed circles represent the hardness of the a-C films (W-group) and the a-C:H films (H-group), respectively.

Table I: Experimental results from EELS and Raman spectroscopy.

Sample	EELS peak position π (eV)	EELS peak position $\pi+\sigma$ (eV)	Raman peak position G-band (cm^{-1})	Raman peak position D-band (cm^{-1})	Raman FWHM G-band (cm^{-1})	Raman FWHM D-band (cm^{-1})	I_D/I_G[a]
W1	5.0	24.6	1541	1368	105	254	2.0
W2	5.6	24.7	1558	1379	142	401	5.7
W3	6.1	24.7	1560	1379	147	394	5.3
W4	6.0	24.4	1562	1378	141	390	6.5
H1	6.3	23.3	1542	1334	95	187	1.6
H2	6.5	23.2	1579	1345	65	172	3.2
H3	6.7	22.4	[f]	[f]	[f]	[f]	[f]
H4	6.5	23.2	[f]	[f]	[f]	[f]	[f]
H5	6.1	22.5	[f]	[f]	[f]	[f]	[f]
H6	5.8	22.0	[f]	[f]	[f]	[f]	[f]
graphite	6.4	27.0	1581	1358	37	47	0.7
diamond	--	37.0	--	--	--	--	--

[a]intensity ratio of the D-band to the G-band.
[f]fluorescence.

Table II: Experimental results of physical properties.

Sample	Electrical resistivity (Ohm cm)	Mass density ($g\ cm^{-3}$)	Hardness (GPa)	Modulus (GPa)
W1	1300	2.1	15	141
W2	2.1	1.9	15	131
W3	0.61	1.8	14	136
W4	0.53	1.8	12	115
H1	--	--	14	96
H2	$\approx 10^5$	--	10	53
H3	$>10^6$	1.7	7	35
H4	$>10^6$	1.6	3	21
H5	$>10^6$	1.6	4	26
H6	$>10^6$	--	6	30
graphite	4×10^{-5}[a]	2.267[a]	--	--
diamond	10^{18}[a]	3.515[a]	≈ 100[a]	--

[a]Data from ref. 43.

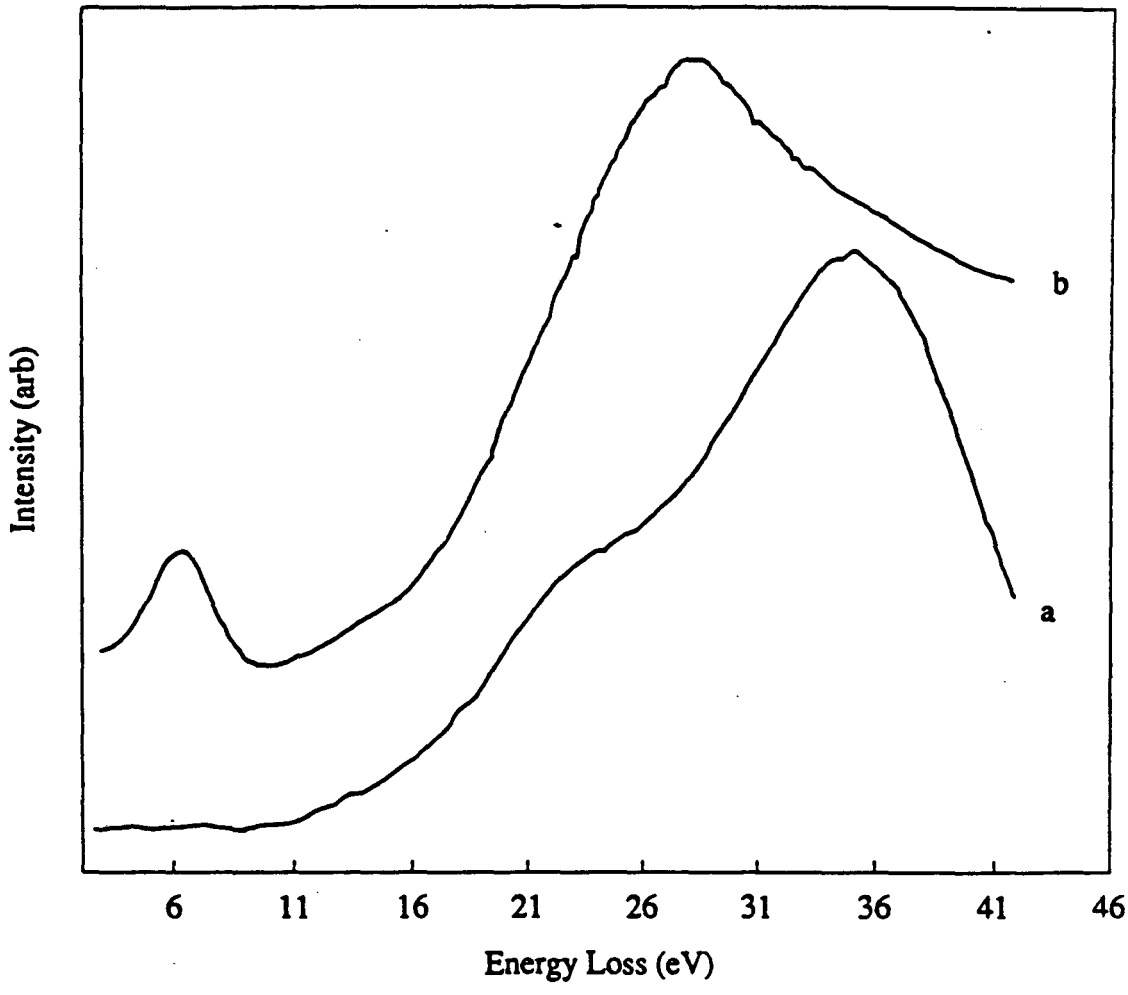

Fig. 1
N.-H. cho et al

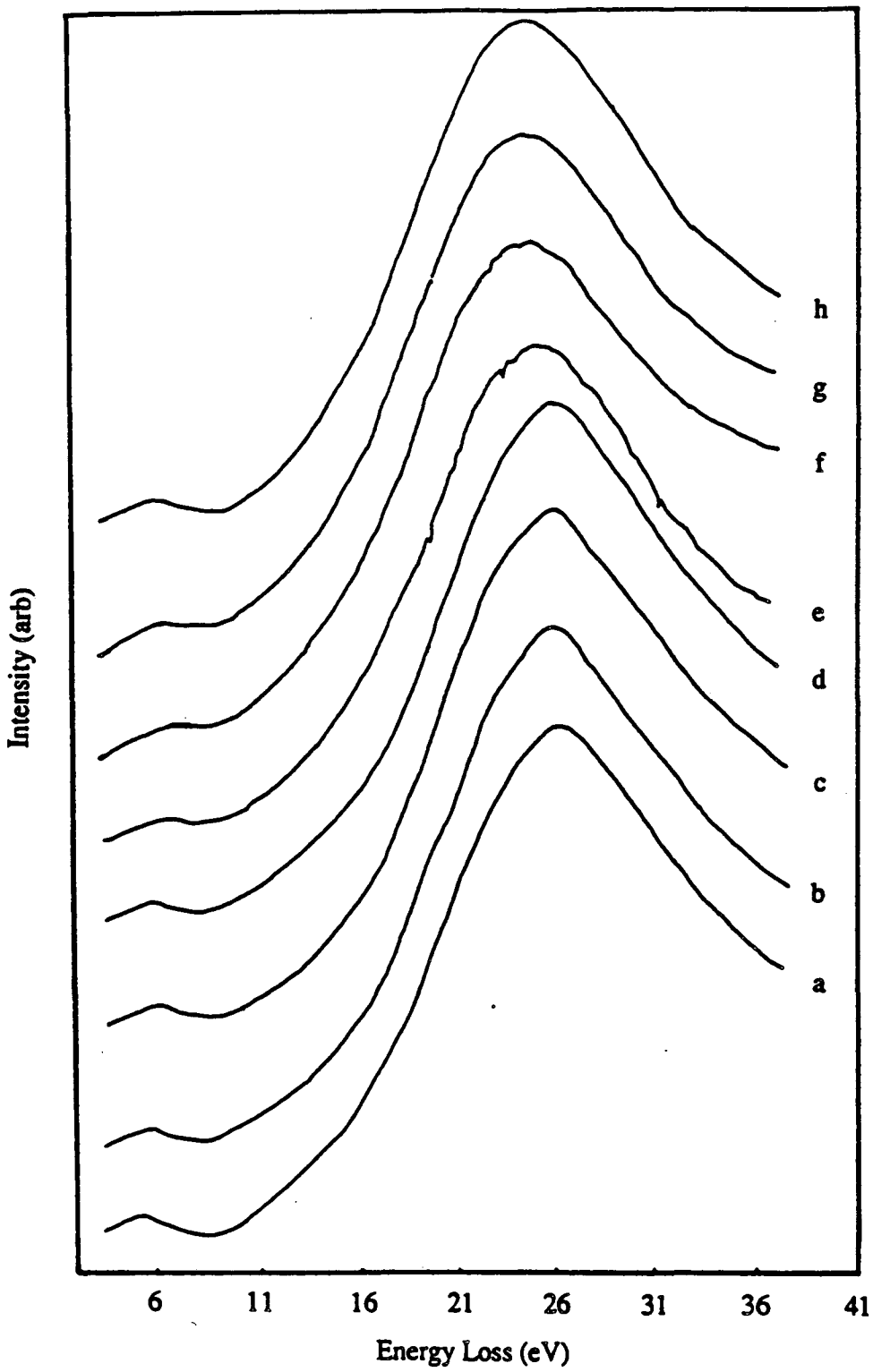
Intensity (arb)
h
g
f
e
d
c
b
a
6
11
16
21
26
31
36
41
Energy Loss (eV)
XBL 904-1324

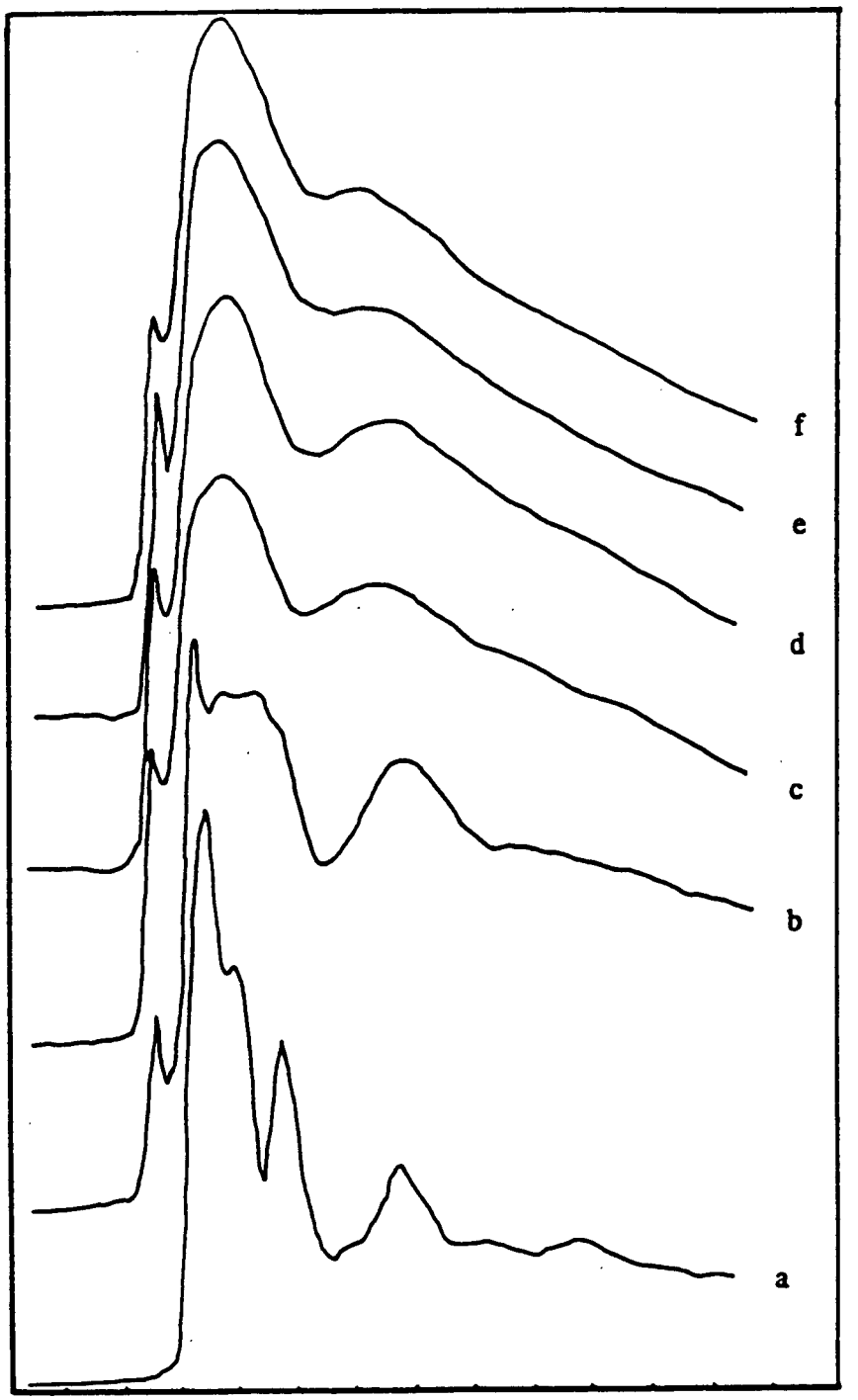

XBL 904-1325

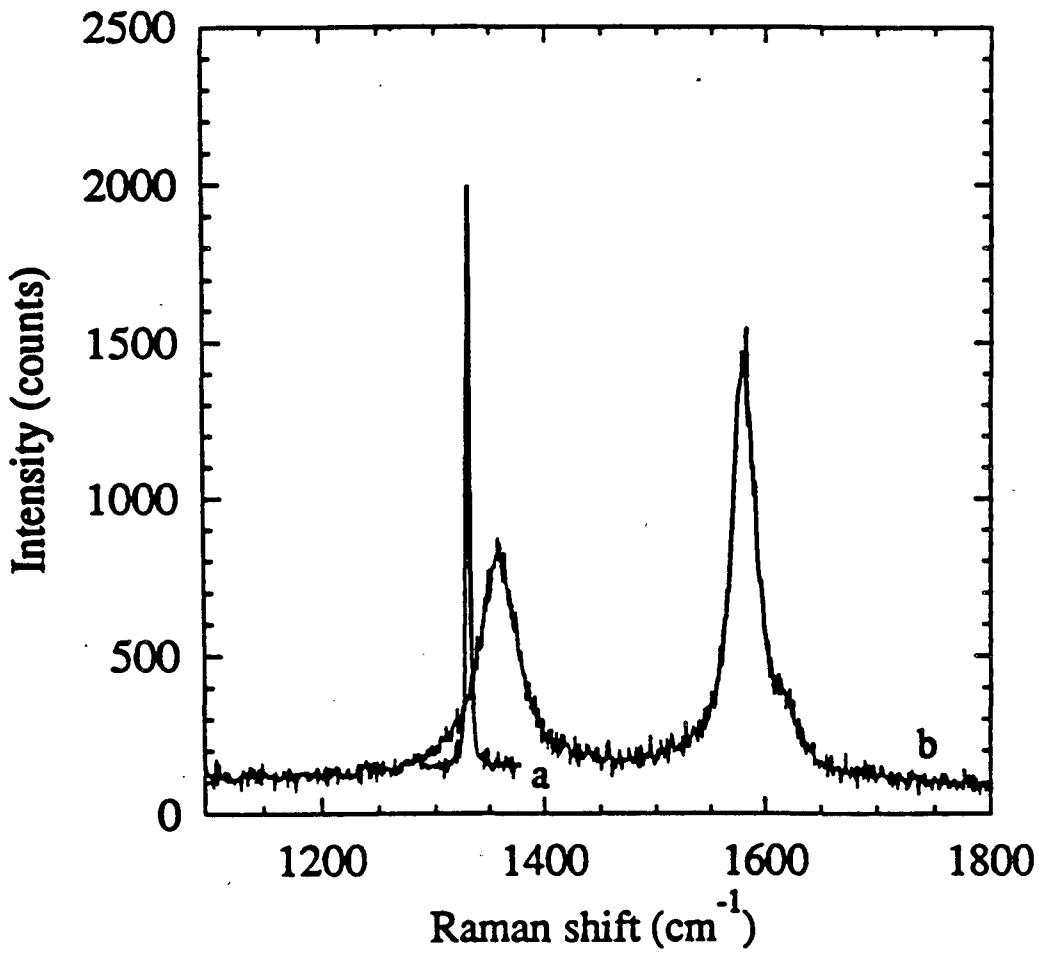

Fig. 4
N.-H. Cho et al

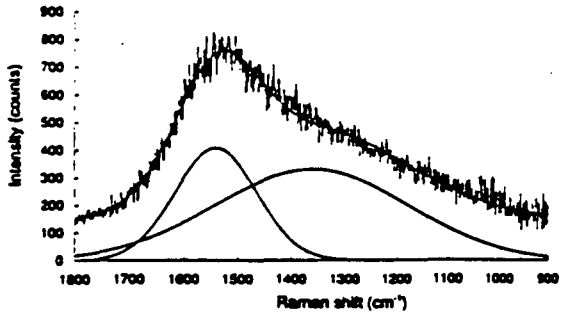

a

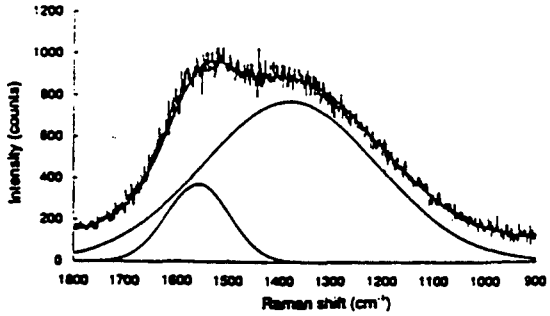

b

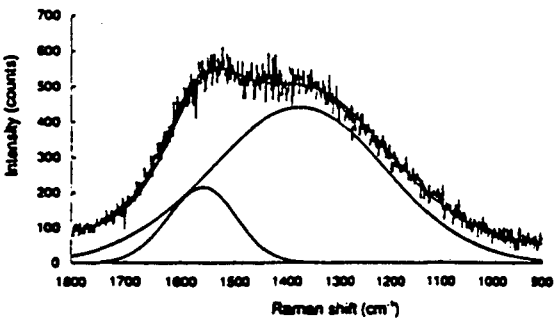

c

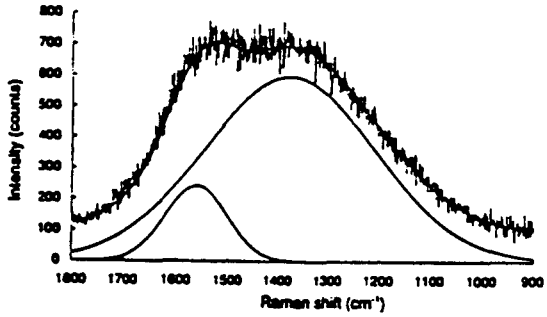

d

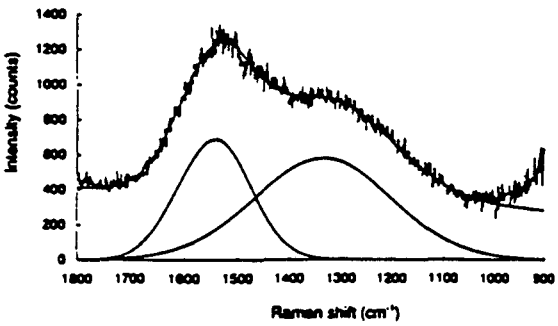

e

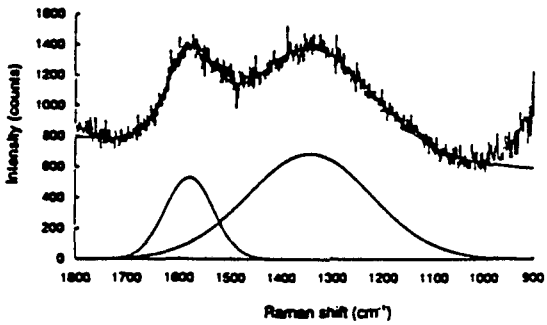

f

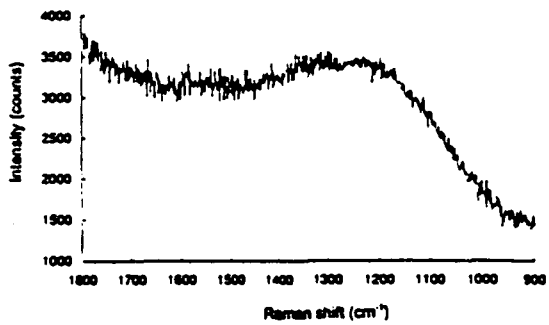

g

XBL 904-1326

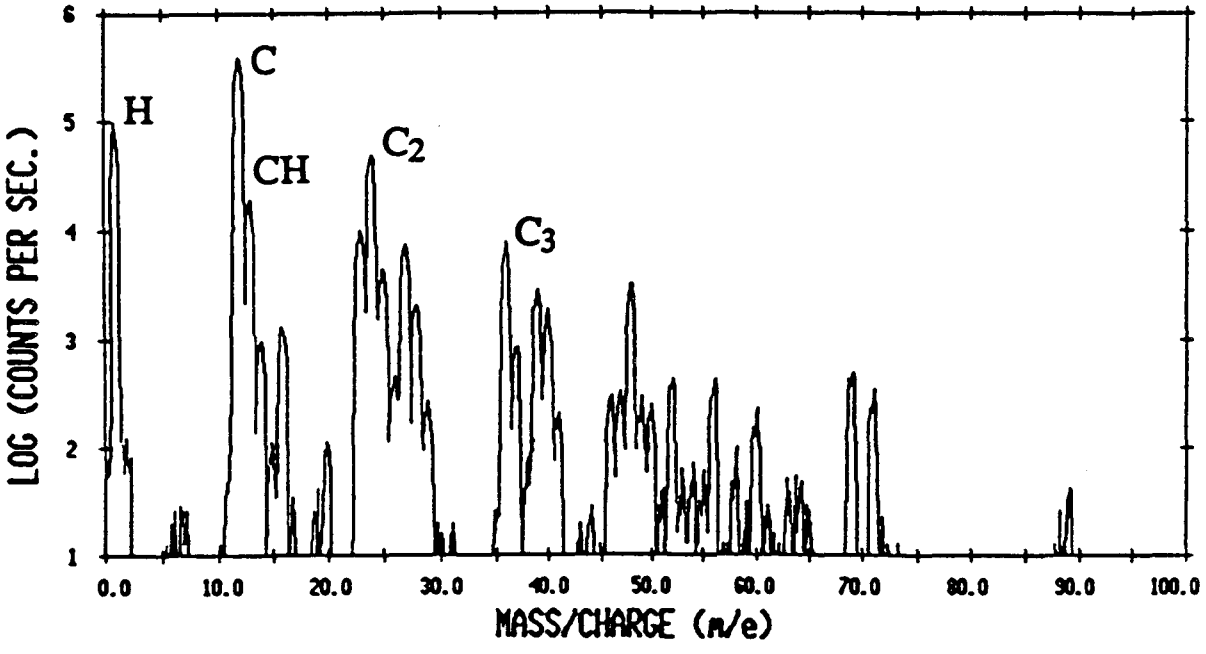
LOG (COUNTS PER SEC.)
MASS/CHARGE (m/e)
H
C
CH
C2
C3
1
2
3
4
5
6
0.0
10.0
20.0
30.0
40.0
50.0
60.0
70.0
80.0
90.0
100.0

XBL 904-1327

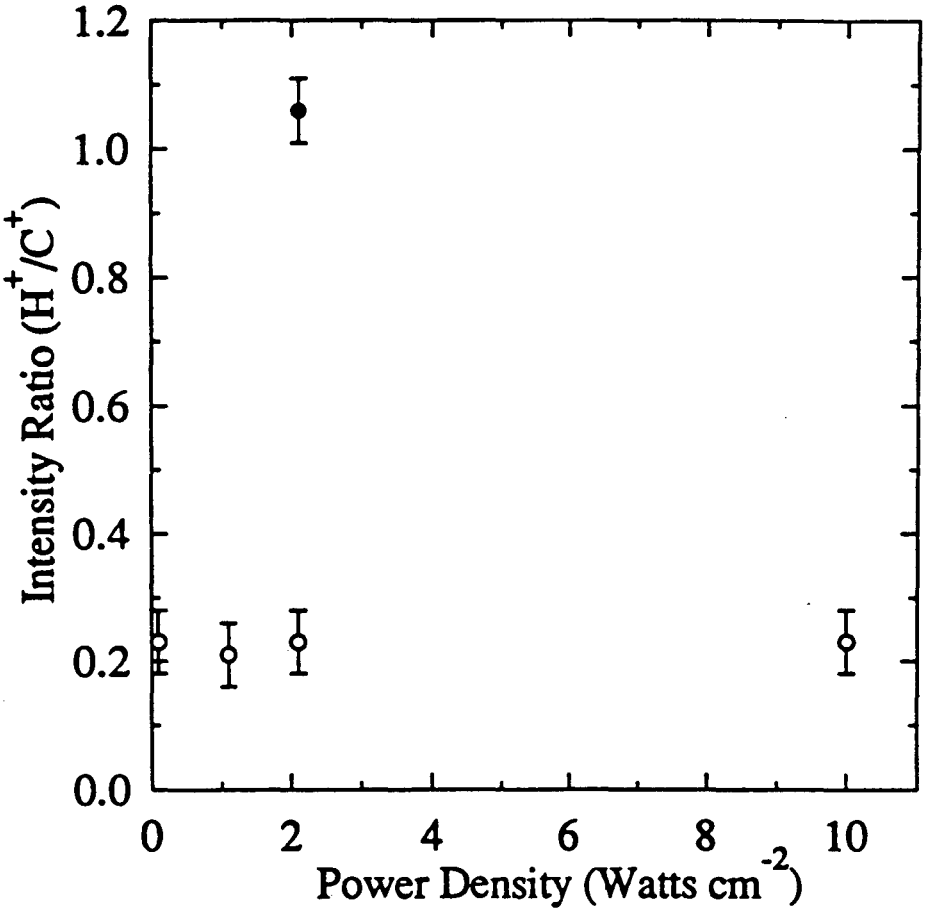

Fig. 6b
N.-H. Cho et al

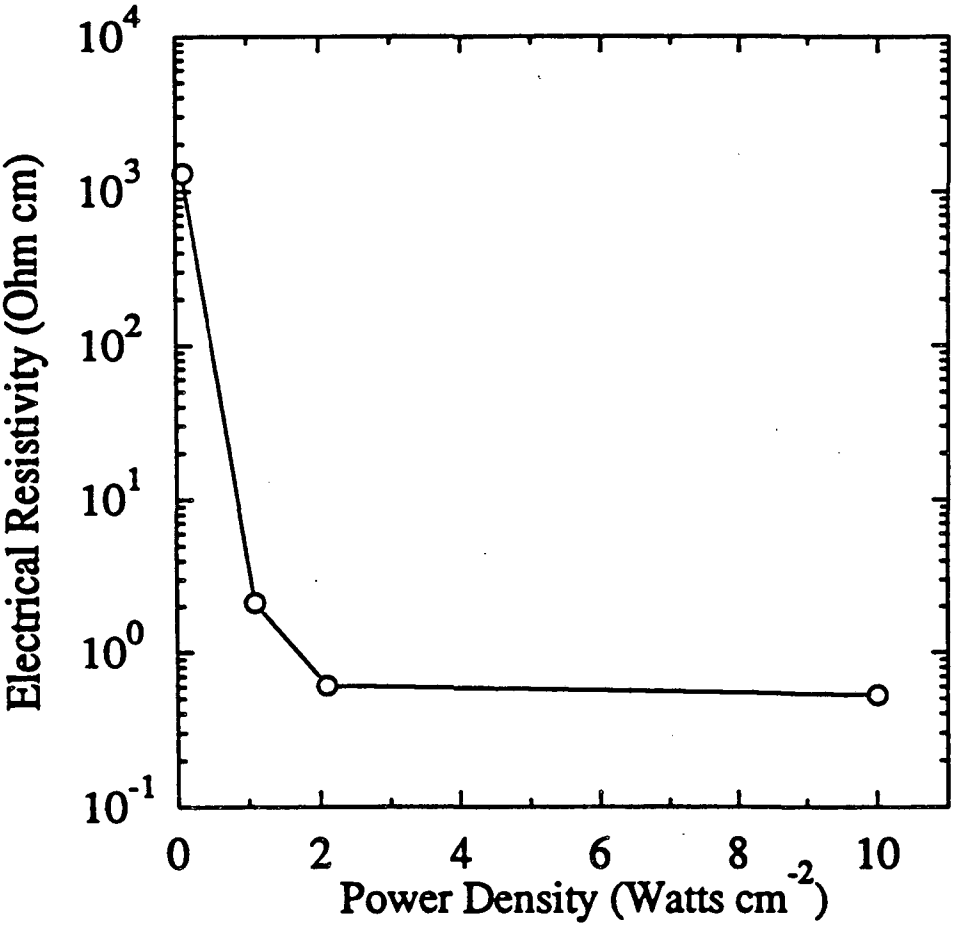

Fig. 7
N.-H. Cho et al

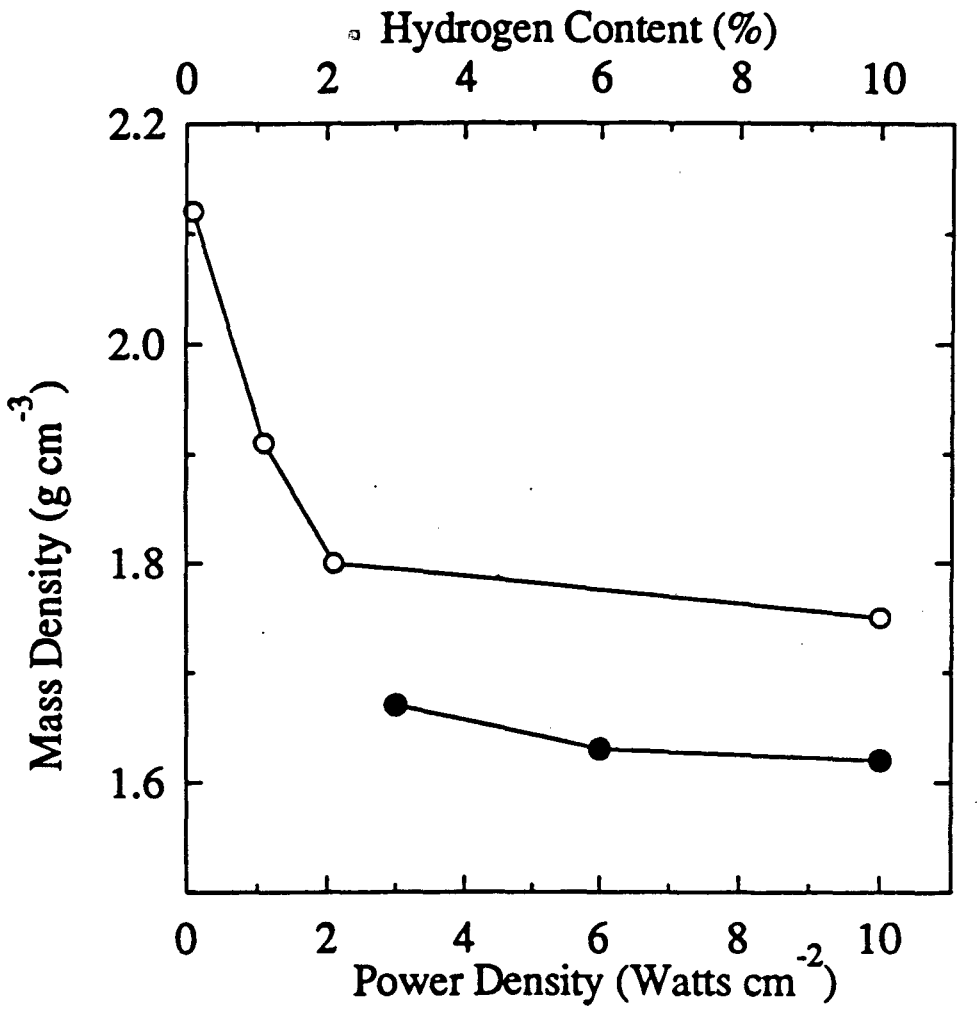

Fig. 8
N.-H Cho et al

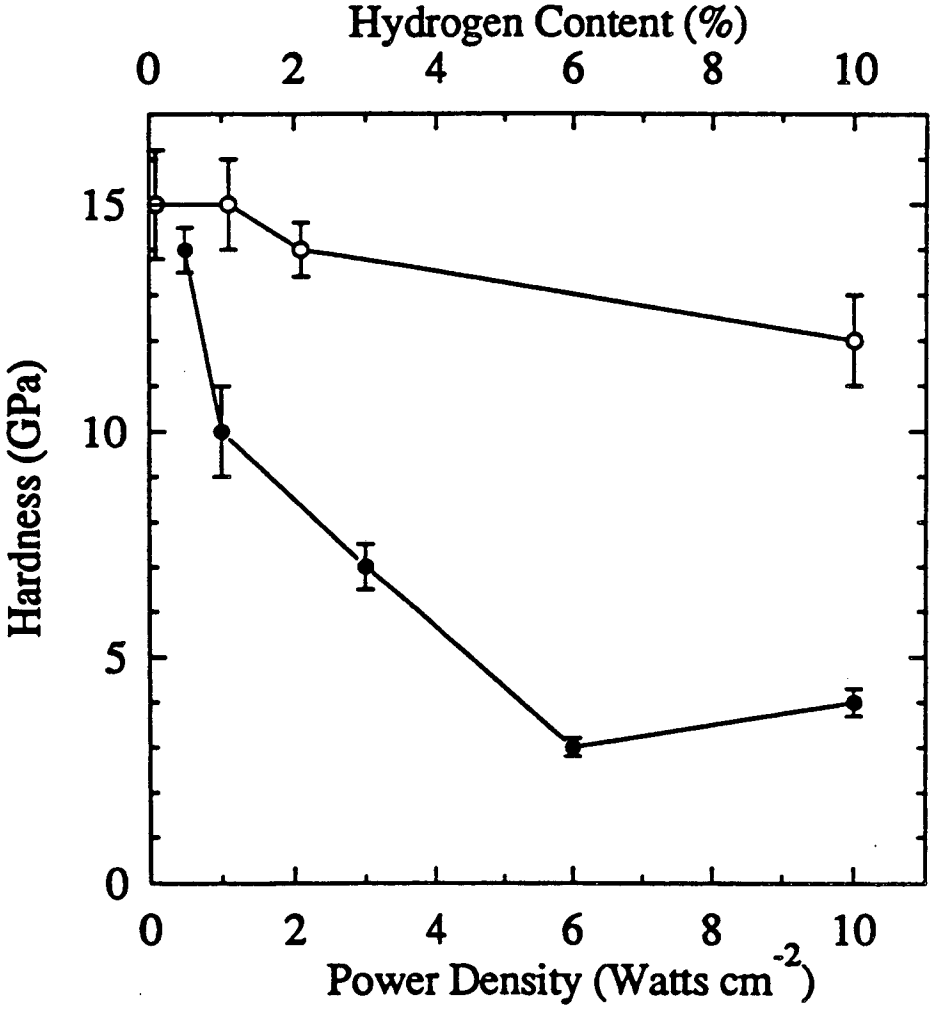

Fig. 9
N.-H Cho et al

LAWRENCE BERKELEY LABORATORY
UNIVERSITY OF CALIFORNIA
INFORMATION RESOURCES DEPARTMENT
1 CYCLOTRON ROAD
BERKELEY, CALIFORNIA 94720